Optical Drills by Dynamic High-Order Bessel Beam Mixing

Gabrielius Kontenis,[1] Darius Gailevičius[◉],[1,2,*] Noé Jiménez[◉],[3] and Kęstutis Staliunas[1,4,5,†]

[1]*Faculty of Physics, Laser Research Center, Vilnius University, Saulėtekio Ave. 10, LT-10223, Vilnius, Lithuania*
[2]*Femtika Ltd, Saulėtekio Ave. 15, LT-10224, Vilnius, Lithuania*
[3]*Instituto de Instrumentación para Imagen Molecular, Centro Mixto CSIC—Universitat Politècnica de València, 46022, València, Spain*
[4]*ICREA, Passeig Lluís Companys 23, 08010, Barcelona, Spain*
[5]*Departamento de Fisica, UPC, Rambla Sant Nebridi 22, 08222, Terrassa, Spain*

One of the key trends in laser material processing is the usage of structured laser beams. Collimated and focused Gaussian beams are the most common tools; however, more exotic beams can be beneficial too. For instance, Bessel beams with elongated focal area and self-healing properties, or vortex beams with helical wave fronts and a dark area along the optical axis are being increasingly used. Here, we propose and experimentally demonstrate dynamical "optical drill" beams presenting nonstationary intensity distributions that resemble a spinning mechanical drill. Optical drills appear as the spatiotemporal interference of two Bessel-vortex beams of different topological charges and different carrier frequencies. By mixing a pair of high-order Bessel beams, synthesized using a liquid crystal spatial light modulator, optical drills of tuned helicities are experimentally observed, and the simplest cases of matter processing (fluorescence) with such beams are demonstrated. Optical drill beams are expected to be useful in material processing by light or in cell and particle manipulation in biomedical applications.

I. INTRODUCTION

In the late 1980s, Durnin and colleagues outlined the concept of Bessel beams—nondiffracting light beams with intriguing properties [1]. Since then, Bessel beams have found applications in many areas, including optical trapping and tweezing, precision drilling of high-aspect-ratio holes [2], and others. A zero-order Bessel beam, given by $E(r, \varphi, z) = A_0 e^{-ik_z z} J_0(k_r r)$, where r and φ are transverse and polar coordinates, z is the coordinate in the propagation direction, and k_z and k_r are the axial and radial components of the wave vector, exhibits azimuthal symmetry, therefore it do not carry orbital angular momentum.

Orbital angular momentum is present in higher-order Bessel beams, $E(r, \varphi, z) = A_0 e^{-ik_z z} J_m(k_r r) e^{im\varphi}$, with azimuthal index $m = 0, \pm 1, \pm, 2, \pm 3 \ldots$, which controls the phase dependence on the azimuthal angle, i.e., the topological charge. As a result, a phase dislocation at the axis is obtained, the beam presents helical wave fronts, and the intensity distribution resembles a hollow tube. The asymptotical radial field distribution around the optical axis depends on the topological charge as $|E(r)| \sim r^m$. Zero- or higher-order Bessel beams have an

advantage over Laguerre-Gauss beams due to the long focal region—infinitely long for ideal Bessel beams (with infinite energy) and relatively long for truncated Bessel beams. Such Bessel beams are useful for imaging, particle manipulation [3–7], communications where information can be encoded using the topological charge [8], microfabrication [9–11], microchannel ablation [12–14], and others. The techniques of Bessel beam formation are already well established. These beams can be generated by circular slits, spiral phase plates [15], conical lenses, i.e., axicons, spatial light modulators (SLMs) [16–18], or computer-generated holograms [19]. Note that Bessel beams of higher order ($|m| > 1$) can be generated by introducing multiple phase jumps $2m\pi$ in angular direction of axicons or, equivalently, by multiarmed spirals in phase masks. For Bessel beams, the phase mask in the simplest case is given by $\varphi = \alpha r/\lambda + m\theta$, where α is the radial phase slope, i.e., the axicon angle. Bessel beams are also known in acoustics, where they are formed using spiral acoustic diffraction gratings [20], metasurfaces [21], or acoustic holograms [22].

Single Bessel beams show a uniform intensity distribution along the propagation direction. However, the superposition of two Bessel beams with different helicities can lead to nontrivial interference patterns, as has been shown in Refs. [23,24]. The propagation wave number

_____

*darius.gailevicius@ff.vu.lt
†kestutis.staliunas@icrea.cat

of a Bessel beam along the optical axis is given by $k_z = \sqrt{k_0^2 - k_r^2}$, where $k_0 = \omega/c = 2\pi/\lambda$ is the wave number and $k_r = k_0 \sin\alpha$. As a result, the propagation wave number k_z depends on the radial phase slope of the axicon and/or mask. Therefore, the interference of two helical beams with different helicities and different axicon angles results in complicated patterns in the angular and radial domains, overall resembling a mechanical drill bit.

In this work, we study the emergence of time-varying helical patterns of light intensity, i.e., *optical drills*, by mixing Bessel beams with different axicon angles, different carrier frequencies, and different topological charges, resulting in a dynamical light pattern that resembles a rotating mechanical drill.

II. RESULTS

A. Synthesis of optical drill beams

Consider first a pair of confocal high-order Bessel beams, formed by different axicon angles, but with the same carrier frequency, as shown in Figs. 1(a) and 1(b). Each beam propagates with a different axial wave vector k_z. Without loss of generality, a convenient way to realize this is to use a circular aperture for the first beam and an annular area for the second, to obtain in this case $k_{z,1} > k_{z,2}$, as shown in Figs. 1(a) and 1(b). Then, if each beam is of a different topological charge, m_1 and m_2, the gradients of the phase along the axial and along the azimuthal directions are different. Therefore, only the points separated by distance d are in phase in the axial direction, where $1/d = |1/d_1 - 1/d_2|$, and

$d_{1,2} = 2\pi/k_{z,1,2}$ are the spatial phase periods of the interfering beams. In addition, only the points separated by azimuthal angle $\varphi = 2\pi/m$, with $m = |m_1 - m_2|$, are in phase in the azimuthal direction. Remembering that each of the components presents an intensity distribution in the form of a hollow tube for $|m_{1,2}| > 0$, the final spatial wave interference pattern of the two beams results in a helical intensity pattern [Fig. 1(c)]. The resulting helical beam is a drill bit with a winding period d. For example, if the topological charges differ by $|m_1 - m_2| = 1$, then the resulting intensity pattern is a single helix, resembling an Ribonucleic acid (RNA) molecule or a corkscrew.

In general, an m-helical beam is obtained, with $m = m_1 - m_2$. For instance, $m = 2$ results in a double intertwined helicoidal beam resembling a DNA molecule or a mechanical drill bit. In addition, by changing the signs of the topological charges, the handedness, i.e., clockwise or counterclockwise, of the intensity profile can be chosen. Evidently, the overlap area of two primary beams must be optimized to match the hollow cylindrical focal areas of both beams. In the example shown here, this can be accomplished by selecting the correct axicon angles, and the geometries of the beams. The conditions for optimal overlapping are explored in Sec. 1 within the Supplemental Material [26].

Up to this point, a static and elongated helical intensity distribution is considered. However, when the two Bessel beams have different carrier frequencies, ω_1 and ω_2, the beams show a different temporal phase variation and, therefore, the resulting interference pattern rotates with time, with an angular frequency given by $\omega = \omega_1 - \omega_2$. Note that the difference can be set positive or negative to obtain clockwise or anticlockwise rotation of the drill bit.
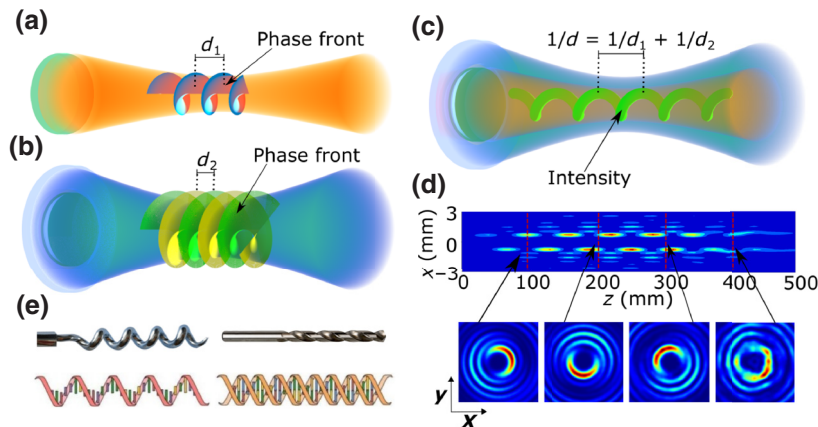

FIG. 1. Generation of optical drill beams. (a) Phase-helical Bessel beam with single-helicity $m_1 = 1$ wave front. (b) Phase-helical Bessel beam with double-helicity $m_2 = 2$ wave front. (c) Optical drill bit, emerging from the interference of beams (a) and (b), showing a helical *intensity* distribution. (d) Axial x-z and transverse x-y cross sections of the simulated intensity distribution. The inner beam of topological charge of $m_1 = 1$ is formed by the axicon with an angle of 0.61°, while the outer beam of $m_1 = 2$ is formed by the axicon of angle 1.04°. (e) Mechanical and biological analogs with the same geometric structure as the proposed light intensity patterns: a corkscrew or RNA molecule for single helicity, and a drill bit or DNA [25].

In general, rotating helix beams emerge as the spatiotemporal interference of the mixed beams because they present a detuned phase gradient in the axial, azimuthal, and temporal domains. In this way, optical drills with highly tunable geometrical parameters, i.e., length, radius, and winding period with an adjustable number of interlaced helixes, and tunable rotation frequency, can be formed.

B. Observation of optical drills

To experimentally demonstrate the generation of optical drills, a setup based on spiral gratings is developed. The mixing of two Bessel beams can be in principle performed in different ways. One possibility is to generate separately two beams of different frequency, and to interfere them by conventional optical means, such as combining imaging optics and beam splitters. In our case, we generate two high-order helical Bessel beams on the same optical component, a phase grating, which consists of two concentric regions, a central disk and an outer annular area, as shown in Fig. 2(a). Each region presents different winding numbers to provide different topological charges, and different radial periods to provide different axicon angles. Specifically, the gratings are generated by a liquid crystal on silicon SLM (HoloEye Photonics AG, Germany), providing high energy reflective efficiency ($>93\%$) and decent diffraction efficiency (approximately 60%), if the generated ramps in the hologram have more than four steps for each 2π phase shift. The SLM is implemented in the setup shown in Fig. 2(b). Here a Nd : YAG laser with a central wavelength of 1064 nm and 10-ns pulse duration is used. The beam is linearly polarized with the help of a $\lambda/2$ plate to align the electric field vector with the slow axis of the liquid crystals of the beam-shaping element. A beam is expanded before the SLM to efficiently use the whole SLM area. A 4F lens system is used to propagate the beam to the final focusing optics without distorting the phase distribution. The final focusing element is used to superimpose different order Bessel beams on top of each other and to achieve interference as in Ref. [27]. The result is observed with a beam profiler CCD camera [Fig. 2(c)].

The next challenge is imparting rotation onto the optical drill bit. A straightforward solution is to project the beams of different frequencies on the inner and outer parts of the phase mask. Note that the two beams must be mutually coherent to give steady rotation of the interference pattern. The mixing from the two separate lasers would give random jumps of the angle of the drills on top of the dominating rotation, with the average time between the jumps equal to mutual coherence time. Our solution is to rotate one grating by a dynamical phase mask, using the SLM in a dynamical regime. The rotation of the helical mask results in a Doppler shift of the frequency in the reflected radiation. The SLM used has a temporal resolution of 60 Hz, allowing a smooth rotation with a frequency of several hertz. The spatial periods and radii of the two parts of the phase mask are adjusted to ensure maximum overlap of the two Bessel beams, and thus maximum intensity contrast of the drill (see Sec. 2 within the Supplemental Material [26]). Note that the drill rotation speed can be increased by rotating both the inner and the outer phase mask areas in opposite directions.

The numerically simulated and experimentally measured intensity patterns are summarized in Figs. 3 and 4. Figure 3(a) shows a simulated helical beam of $m_1 = 4$ and $m_2 = 8$, where xy intensity cross sections at different axial distances are indicated in Fig. 3(b). The final spiral structure has a number of arms equal to
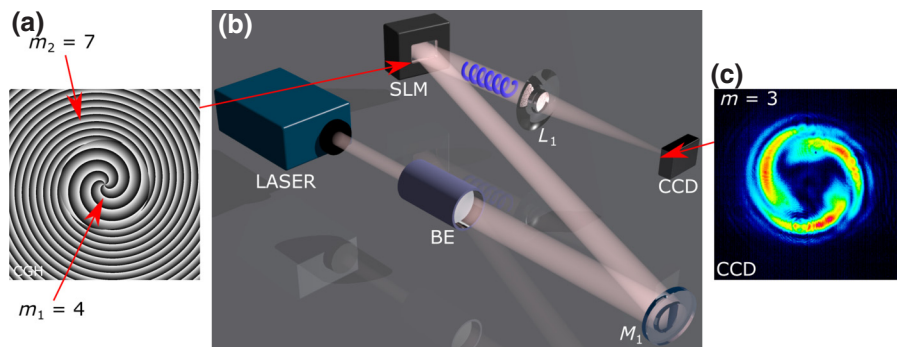

FIG. 2. Optical scheme used for beam shaping. (a) Grayscale phase image of a computer-generated hologram (CGH) displayed on the SLM. Black areas correspond to a phase shift of 0, whereas white areas correspond to 2π. Central Bessel with $m_1 = 4$; outer Bessel with $m_2 = 7$. The inner Bessel disk diameter is calibrated to approximately equally divide the initial Gaussian beam energy. (b) The incoming laser beam is expanded via using the beam expander (BE) to reduce the power density and effectively use the active SLM area. A half-wave plate is used to align the laser polarization with the nematic liquid crystals of the SLM. A beam is focused on a CCD camera for visualization. A 4F system comprised of two lenses can be used to relay the phase front from the SLM plane to the final focusing objective input pupil plane in systems. (c) The intensity distribution measured on the CCD camera of the spatially modulated beam.
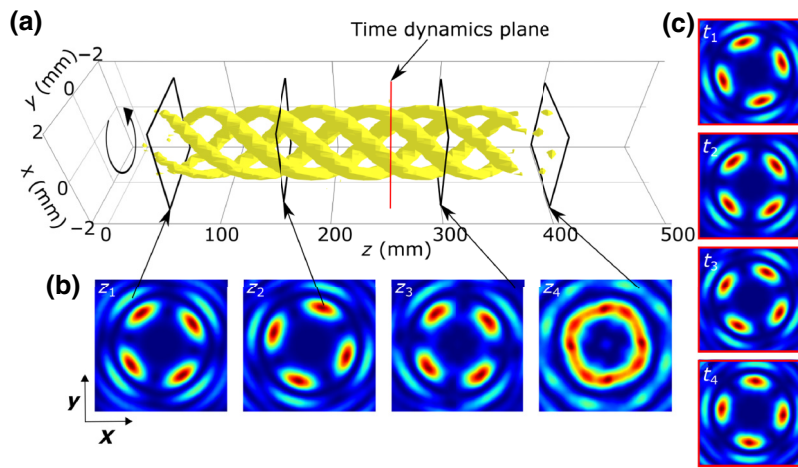
FIG. 3. Numerical simulation of the evolution of the optical drill. (a) 3D isosurface model of the interference of two Bessel-Gauss beams creating the spiral intensity structure—optical drill. The figure shows a four-arm optical drill formed by two Bessel beams of $(m_1 = 4, m_2 = 8)$. (b) Simulated x-y cross-section intensity distributions at different planes. Full propagation of a three-arm variant is given in Video 1 within the Supplemental Material [26]. (c) Simulated intensity distribution x-y cross sections rotating in time recorded from a single plane (indicated in red). Numerical simulation and full rotation of the simulated three-arm drill are given in Video 2 and Sec. 3 within the Supplemental Material [26].

the difference in the topological charge of the interfering Bessel beams; in this particular example, an $m = +4$ helical structure is observed. The whole structure is rotating in time [Fig. 3(c)]. In addition, experimentally, various topological charges are produced (Sec. 4 within the Supplemental Material [26]) and dynamical optical drill is given in Fig. 4. Both cases show that the higher the Bessel beam order, the broader the central hollow area. This is due to the individual interfering Bessel beams having large ring diameters in the far field. Additional secondary spirals, with lower intensity, are visible in the simulated optical drills due to the interference of Bessel components not yet intersecting on the optical axis.

The experimental case has some interesting properties. First is the diverging shape depending on the precise placement of the focusing lens. Second, the winding period is changing along the z axis. This is expected as the whole Bessel zones for both beams are comparable in length with the relevant lens focus. This can be understood via an effect like "spherical aberration" [28], where the addition of the lens modulates the propagation angle for rays with different radial offsets from the optical axis. Such an effect is not accounted for in the numerical model as propagation distances cannot be comparable due to resolution limitations (angle versus resolution trade-off).

The total size of optical drill beams is determined by the axicon angles. Further magnification can be done by employing an imaging setup comprised of a pair of lenses (an expanding telescope). The total number of windings in

the drill, as estimated in Sec. 5 within the Supplemental Material [26], is

$$N = \frac{r_1}{2\lambda} \frac{(\alpha_2 - \alpha_1)^2(\alpha_1 + \alpha_2)}{\alpha_1\alpha_2}. \tag{1}$$

Here $D_\parallel$ is the length of the axial overlap area of the inner and outer Bessel beams and r_1 is the radius of the inner part of the hologram. In terms of the number of windings of the internal part of the hologram $m = r_1\alpha_1/\lambda$, and in terms of ratio of axicon angles $\alpha = \alpha_2/\alpha_1$, we finally obtain a simple estimation:

$$N = m(\alpha - 1)^2(\alpha + 1)/(2\alpha). \tag{2}$$

In this way, optical drills are realized with highly tunable geometrical parameters, i.e., length, radius, and winding period, adjustable number of staggered helixes, and tunable rotation frequency. In Sec. 6 within the Supplemental Material [26], different optical drills with different parameters are shown.

C. Interaction with matter

The drill is expected to interact with material primarily through a thermal effect (during relatively slow rotation of several hertz) and through phonon excitation (during fast rotation of several kilohertz). Possibly fast rotation (megahertz and gigahertz ranges) can result in interesting interaction effects; however, a detailed analysis of wave-matter interaction is out of the scope of the article. As a proof of concept, we present here the interaction of the optical
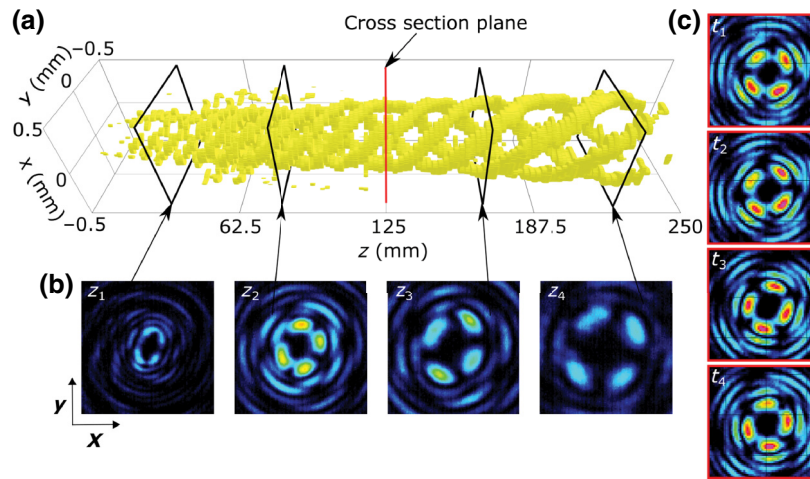
FIG. 4. Experimental observation of an optical drill. (a) 3D isosurface of an experimentally realized interference of two Bessel-Gauss beams creating spiral intensity structure. A four-arm optical drill ($m = 4$) formed by the superposition of two Bessel beams with topological charges $m_1 = 4$ and $m_2 = 8$. (b) Measured intensity distribution at different axial distances. The separation between slices is 70 mm and the focal length of the used lens is 150 mm. (c) Optical intensity in the indicated cross section as a function of time, showing the rotation of the optical drill. A frequency of 6 Hz is set taking into account beam symmetry (1.5 Hz for a full 360° rotation). See Video 3 within the Supplemental Material [26] for three-arm dynamic data.

drill focused inside a Rhodamine B dye [see Fig. 5(a)]. For this experiment, a separate 532-nm-wavelength laser is used to enhance the material fluorescence. Due to the aspect ratio of the optical drill, magnifying optics are used to scale the beam itself and, in addition, an imaging microscope comprised of a microscope objective and lens is used for a more detailed image. The sense of winding in the propagation direction and its rotation speed are adjusted by changing the rate at which computer-generated holograms are displayed on the SLM. Fluorescence emission is imaged at different times, as shown by the snapshots in Fig. 5(b). The fluorescence images match the time-varying beam structure of the optical drill, showing the winding of a helical structure of $m = 2$ arms inside the fluorophore. By selecting different rotation frequencies, the helical beam rotation direction can be selected, as shown in Video 4 and Video 5 within the Supplemental Material [26]. Therefore, the interference pattern of the optical drill beam is shown to move in a forward or backward direction inside the fluorescent medium.

III. CONCLUSIONS

Light beams with rotation-in-time helical intensity distribution, rotating optical drills, emerge as the spatiotemporal interference of high-order Bessel beams with different axicon angles, different topological charges, and different carrier frequencies. The parameters of the optical drills, i.e., length, radius, and winding period, and the order of helical structure are highly tunable. In addition, the rotation frequency and sense of rotation of the drill can be set by adjusting the frequency detuning. In this work,

we experimentally demonstrate the main features of these beams using the interference of two beams on a rotating SLM, and its interaction with matter through fluorescence. Note that, while the rotation of the SLM hologram is sufficient to demonstrate the principle, the rotation frequency possibly must be strongly increased for technologically relevant applications, e.g., using acousto-optical devices to obtain two coherent Bessel beams of coherently different frequencies. It is also worth noting here that, while the use of high-order Bessel beams leads to elongated and regular helical structures, as demonstrated here, optical drills can be generated by mixing any pair of overlapping and detuned vortex beams.

Like the case of stationary helical beams [29–33], the optical drill could become a tool for particle micromanipulation. Moreover, its rotation in time can add the possibility of attracting or pushing particles along the optical axis. Most likely the temperature gradients induced on the material during laser processing from the rotating intensity maxima. This article shows the main principle of the optical drill, experimental observations, and evidence of interaction with matter, but further studies should show the features of drills for optomechanical processing of matter using pulses with higher energy. Dynamic programmable beam shaping can be effectively used for microfabrication and reduce processing time. We hope that these dynamical light structures can bring a revolution to emerging optical technologies for matter processing, as the invention of mechanical drills brought a revolution in construction technologies as compared with previously dominant nails in constructions.
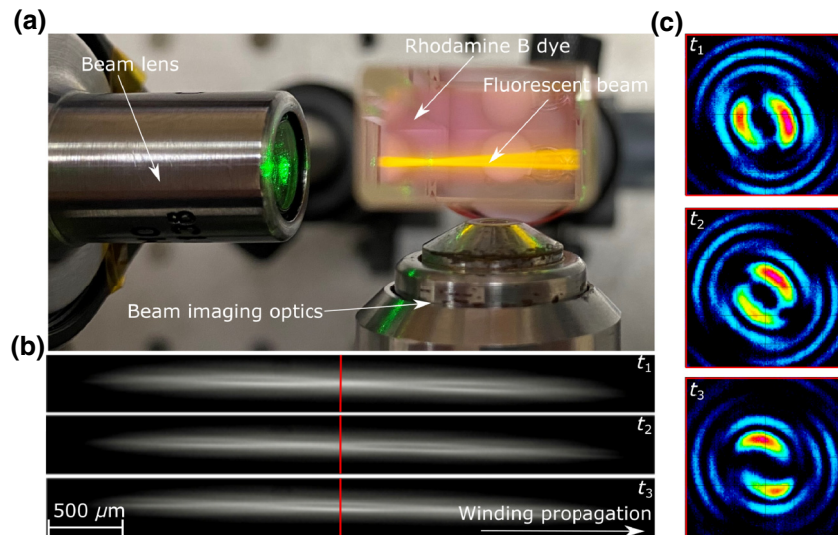
FIG. 5.   Optical drill experimental fluorescence visualization. (a) Fluorescence of the Bessel-Gauss interference pattern captured in Rhodamine B dye. (b) An enlarged fraction of the full optical drill at different times. (c) Transverse intensity profiles of the rotating optical drill beam with $m = 2$, i.e., a double helix, at different times.

APPENDIX A: METHODS

1. Numerical simulations

Simulation codes are written in Python using an iterative Fourier split-step propagation method. An initial Gaussian amplitude beam is used, whose initial phase distribution is modified by an axicon grating and an azimuthally varying phase offset or a spiral phase plate. The beam is propagated by a small step in the Fourier plane, and the inverse Fourier transform is taken, to get the current intensity distribution in the real plane. All planes are assembled and a three-dimensional (3D) isosurface structure is reconstructed of the simulated beam.

2. Three-dimensional experimental generation

For 3D reconstruction and beam generation experiment, a HoloEye Pluto 2.1 NIR-149 liquid crystal SLM with 8-μm pixel pitch, 93% fill factor, and 60-Hz refresh rate is used. The laser source is a Nd : YAG passively q-switched DPSS laser WG077-E-1 with 1-ns pulse width and 100-Hz repetition rate. Because the SLM only works with linearly polarized light, a half-wave plate is used to align the linear polarization to the SLM liquid crystal axis. A beam expander comprised of two lenses, -50 and 200 mm, is used to expand the beam and more efficiently use the SLM active area. The beam size is 7 mm at $1/e^2$. For beam measurements, the diverging Bessel rings are refocused with a 150-mm lens placed 150 mm from the SLM screen into a WinCamD DataRay FIR2-16-HR CCD camera with a 4.4-μm pixel pitch. The CCD camera is translated on a motorized stage and two-dimensional (2D) slices are captured of the optical drill. The collection of slices is collected and parts of the beam with higher intensity are left for a clearer (less noisy) reconstruction of the 3D isosurface.

3. Fluorescence experiment

Rhodamine B dye is used as a fluorescent medium. The initial Rhodamine B powder is dissolved in distilled water to a concentration of 8.26 μg/ml. As the source, a green 532-nm diode laser is used. For dynamic beam shaping a HoloEye LCOS-SLM LC-R-2500-1 designed for 532-nm light with 19-μm pixel pitch is utilized. To have more windings visible in the field of view, a telescope of two lenses is used to compress the beam: 200-mm lens and LOMO $8 \times$ 0.2NA objective. For visualization of the resultant interference beam, a microscope comprised of LOMO $40 \times$ 0.65NA and 100-mm lens is placed on the side and viewed with a Point Grey Chameleon CMLN-13S2M digital camera. An orange glass filter is used to cut off the initial green light of the excitation beam.

[1] J. Durnin, J. Miceli, and J. H. Eberly, Diffraction-Free Beams, Phys. Rev. Lett. 58, 1499 (1987).

[2] M. Duocastella and C. B. Arnold, Bessel and annular beams for materials processing, Laser Photonics Rev. 6, 607 (2012).

[3] G. S. Sokolovskii, S. N. Losev, K. K. Soboleva, V. V. Dudelev, A. G. Deryagin, W. Sibbett, V. I. Kuchinskii, and E. U. Rafailov, Manipulation of microparticles using bessel beams from semiconductor lasers, Tech. Phys. Lett. 40, 475 (2014).

[4] S. H. Tao, W. M. Lee, and X.-C. Yuan, Dynamic optical manipulation with a higher-order fractional bessel beam generated from a spatial light modulator, Opt. Lett. 28, 1867 (2003).

[5] D. McGloin, V. Garcés-Chávez, and K. Dholakia, Interfering bessel beams for optical micromanipulation, Opt. Lett. 28, 657 (2003).

[6] T. A. Planchon, L. Gao, D. E. Milkie, M. W. Davidson, J. A. Galbraith, C. G. Galbraith, and E. Betzig, Rapid three-dimensional isotropic imaging of living cells using bessel beam plane illumination, Nat. Methods 8, 417 (2011).

[7] D. G. Grier, A revolution in optical manipulation, Nature 424, 810 (2003).

[8] S. Li and J. Wang, Adaptive free-space optical communications through turbulence using self-healing bessel beams, Sci. Rep. 7, 1 (2017).

[9] S. J. Zhang, Y. Li, Z. P. Liu, J. L. Ren, Y. F. Xiao, H. Yang, and Q. Gong, Two-Photon polymerization of a three dimensional structure using beams with orbital angular momentum, Appl. Phys. Lett. 105, 061101 (2014).

[10] W. Cheng and P. Polynkin, Micromachining of borosilicate glass surfaces using femtosecond higher-order bessel beams, J. Opt. Soc. Am. B 31, C48 (2014).

[11] S. Mitra, M. Chanal, R. Clady, A. Mouskeftaras, and D. Grojo, Millijoule femtosecond micro-bessel beams for ultra-high aspect ratio machining, Appl. Opt. 54, 7358 (2015).

[12] X. Yu, C. A. Trallero-Herrero, and S. Lei, Materials processing with superposed bessel beams, Appl. Surf. Sci. 360, 833 (2016).

[13] F. Courvoisier, J. Zhang, M. K. Bhuyan, M. Jacquot, and J. M. Dudley, Applications of femtosecond bessel beams to laser ablation, Appl. Phys. A: Mater. Sci. Process. 112, 29 (2013).

[14] M. K. Bhuyan, F. Courvoisier, P.-A. Lacourt, M. Jacquot, L. Furfaro, M. J. Withford, and J. M. Dudley, High aspect ratio taper-free microchannel fabrication using femtosecond bessel beams, Opt. Express 18, 566 (2010).

[15] D. Mcgloin and K. Dholakia, Bessel beams: Diffraction in a New light, Contemp. Phys. 46, 15 (2005).

[16] J. Wu, Z. Wu, Y. He, A. Yu, Z. Zhang, Z. Wen, and G. Chen, Creating a nondiffracting beam with Sub-diffraction size by a phase spatial light modulator, Opt. Express 25, 6274 (2017).

[17] A. Marzo, A. Ghobrial, L. Cox, M. Caleap, A. Croxford, and B. W. Drinkwater, Realization of compact tractor beams using acoustic delay-lines, Appl. Phys. Lett. 110, 014102 (2017).

[18] C. G. Durfee, J. Gemmer, and J. V. Moloney, Phase-only shaping algorithm for Gaussian-apodized bessel beams, Opt. Express 21, 15777 (2013).

[19] I. Ouadghiri-Idrissi, R. Giust, L. Froehly, M. Jacquot, L. Furfaro, J. M. Dudley, and F. Courvoisier, Arbitrary shaping of on-axis amplitude of femtosecond bessel beams with a single phase-only spatial light modulator, Opt. Express 24, 11495 (2016).

[20] N. Jiménez, V. J. Sánchez-Morcillo, R. Picó, L. M. Garcia-Raffi, V. Romero-Garcia, and K. Staliunas, High-order acoustic bessel beam generation by spiral gratings, Phys. Procedia 70, 245 (2015).

[21] H. Esfahlani, H. Lissek, and J. R. Mosig, Generation of acoustic helical wavefronts using metasurfaces, Phys. Rev. B 95, 024312 (2017).

[22] S. Jiménez-Gambín, N. Jiménez, J. M. Benlloch, and F. Camarena, Generating bessel beams with broad depth-of-field by using phase-only acoustic holograms, Sci. Rep. 9, 20104 (2019).

[23] R. Vasilyeu, A. Dudley, N. Khilo, and A. Forbes, Generating superpositions of higher–order bessel beams, Opt. Express 17, 23389 (2009).

[24] S. Zheng, Y. Cai, Y. Li, J. Li, G. Zheng, H. Chen, and S. Xu, Rotating wave packet caused by the superposition of two bessel-gauss beams, J. Opt. 17, 125602 (2015).

[25] S. Aryal, 30 Differences between DNA and RNA (DNa vs RNA), https://microbenotes.com/differences-between-dna-and-rna/.

[26] See Supplemental Material at http://link.aps.org/supplemental/10.1103/PhysRevApplied.17.034059 for additional details and video simulations.

[27] S. Chávez-Cerda, E. Tepichin, M. A. Meneses-Nava, G. Ramirez, and J. M. Hickmann, Experimental observation of interfering bessel beams, Opt. Express 3, 524 (1998).

[28] V. N. Belyi, L. I. Kramoreva, M. K. Al-Muhanna, and N. A. Khilo, Focusing bessel beams by a lens with strong spherical aberrations, Int. J. Opt. 2012, 739413 (2012).

[29] A. Marzo, M. Caleap, and B. W. Drinkwater, Acoustic Virtual Vortices with Tunable Orbital Angular Momentum for Trapping of Mie Particles, Phys. Rev. Lett. 120, 44301 (2018).

[30] K. Volke-Sepulveda, V. Garcés-Chávez, S. Chávez-Cerda, J. Arlt, and K. Dholakia, Orbital angular momentum of a high-order bessel light beam, J. Opt. B: Quantum Semiclassical Opt. 4, S82 (2002).

[31] S. H. Simpson and S. Hanna, Orbital motion of optically trapped particles in laguerre–Gaussian beams, J. Opt. Soc. Am. A 27, 2061 (2010).

[32] S. Chávez-Cerda, M. J. Padgett, I. Allison, G. H. C. New, J. C. Gutiérrez-Vega, A. T. O'Neil, I. MacVicar, and J. Courtial, Holographic generation and orbital angular momentum of high-order mathieu beams, J. Opt. B: Quantum Semiclassical Opt. 4, S52 (2002).

[33] D. P. Rhodes, D. M. Gherardi, J. Livesey, D. McGloin, H. Melville, T. Freegarde, and K. Dholakia, Atom guiding along high order laguerre–Gaussian light beams formed by spatial light modulation, J. Mod. Opt. 53, 547 (2006).